

Pre-design of Diamond Turned  
Refractive/Diffractive Elements for IR Objectives

Max J. Riedl

OFC Diamond Turning Division  
69 Island Street, Keene, NH 03431

### ABSTRACT

Diffractive lenses have arrived. Literally hundreds of papers have been published<sup>1-25</sup> and technology impact reports have been written about the exciting addition of a new tool for the lens designer.<sup>1</sup> Sophisticated computer programs have been developed to aid in the optimization of these diffractive phase profiles for a wide variety of applications. Now, several fabrication methods are being pursued to produce these diffractive elements economically. The best known process is the etching of a multi-level relief grating, known as binary optics.<sup>2</sup> This process uses sets of computer generated lithographic masks. Another, more recently developed method is Dry Photopolymer Embossing (DPE).<sup>3</sup> This replication process uses master holograms. And now, diamond turning is being applied for the machining of these elements.<sup>4,5</sup> Diamond turning is especially well suited for infrared optics. As any process has advantages and limitations, so has diamond turning. These advantages and limitations are discussed and general guidelines are presented to aid the designer and systems engineer in the project pre-design stage.

### 1. INTRODUCTION

Diamond turning is a well established fabrication process for shaping high quality optical surfaces on metals, polymers and crystals. It is therefore a natural extension to apply this proven process to generating surface relief phase profiles of diffractive lenses. The ability to guide a single point cutting tool along a predetermined path to an accuracy of a fraction of one wavelength of light makes this process very suitable for this task. The surface finish achieved with diamond turning is of a quality generally acceptable for optical components for the mid- and long wavelength regions of the infrared spectrum.

### 2. GENERAL REMARKS TO DIAMOND TURNING DIFFRACTIVE SURFACES

Besides material limitations, an important factor that determines the practicality of diamond turning diffractive surfaces is the number of annular zones (modulo  $2\pi$ ) required for a given application. A single point cutting tool has a relatively large radius which is optimized for achieving an acceptable surface finish in a reasonable time. For machining a diffractive surface, this radius should be small to reduce the "shadowing" effect at the transition step from one zone to the next. Much of this paper will address this effect since it is central to the practicality of diamond turning diffractive surfaces.

### 3. THE PHASE PROFILE FUNCTION

$$\varphi(r) = \frac{2\pi}{\lambda_0} [Ar^2 + Br^4 + Cr^6 + \dots] \quad (1)$$

This is the well known function for a rotationally symmetric lens surface with  $r$  being the radial coordinate of the profile,  $\lambda_0$  the wavelength of interest, and  $A, B, C$  etc. the phase profile coefficients. Their optimum values are determined with computer programs such as CODE V, OSLO and ACCOS. For preliminary evaluation it is worthwhile to truncate this expression and examine the resulting approximations. This is being done in the following sections with the assumption that the object is located at infinity.

### 4. THE MONOCHROMATIC SINGLET

A spherical wave front exiting a lens can be expressed by

$$\varphi(r) = \frac{2\pi}{\lambda_0} \left[ -\frac{r^2}{2F} + \frac{r^4}{8F^2} - \dots \right] \quad (2)$$

By comparison with equation (1) it can be seen that

$$A = -\frac{1}{2F} \quad (3)$$

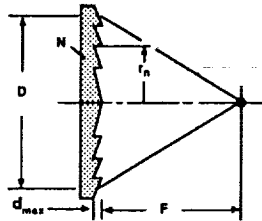
where  $F$  is the focal length of the lens. The negative sign indicates the direction of the phase profile.

The first zone radius, where the  $2\pi$  transition (one wavelength) occurs is therefore at

$$r_1 = \sqrt{2\lambda_0 F} \quad (4)$$

Others occur at

$$r_n = r_1 \sqrt{n} \quad (5)$$



Where  $n$  is the zone number. At the limit  $r_n = D/2$ , with  $D$  being the lens diameter.

The total required zones can now be determined from

$$n_{TOT} = \frac{D^2}{8\lambda_0 F} = \frac{F}{8\lambda_0 (F/\#)^2} \quad (6)$$

Example 1 :

For a lens with  $F = 25$  mm,  $F/\# = 2$ , and  $\lambda_0 = 0.6328$   $\mu\text{m}$ , we find that approximately 1,235 zones are required to achieve the focusing effect.

A more accurate number, which could be obtained from

$$n_{\text{TOT}} = \frac{F}{2\lambda_0 (F/\#)} [\sqrt{1 + 4 (F/\#)^2} - 2 (F/\#)] \quad (7)$$

is 1,216. Notice that the first approximation is within 1.6 % which indicates the value of simplicity.

From the expression

$$d_{\text{MAX}} = \frac{\lambda_0}{(N-1)} \quad (8)$$

we find the maximum depth of a zone at the transition, with  $N$  being the index of refraction of the substrate material.

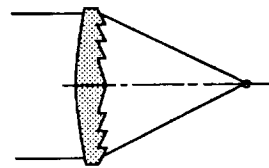
If the material used in the example is plastic, with an index of 1.527, the depth would be approximately 1.2  $\mu\text{m}$ .

## 5. THE MONOCHROMATIC HYBRID SINGLET

Hybrid is defined here as the combination of refractive and diffractive powers within one element. An interesting case is a convex plano lens for which the basic power is provided by the spherical shape of the first surface and the correction of the spherical aberration is achieved with a diffractive phase profile on the second surface.

Considering third order aberration only, one can express the longitudinal spherical aberration for a thin convex plano lens by <sup>6</sup>

$$W_{\text{SPH}} = \frac{[N^2(N-2) + 2] F}{128 \lambda_0 N (N-1)^2 (F/\#)^4} \quad (\text{wavelengths}) \quad (9)$$



Example 2 : For the same basic lens from example 1, now shaped as a convex plano, we find from equation (9) that  $W_{\text{SPH}} = 41$  waves. This means that 41 zones are required to correct 3rd order spherical aberration, since one wavelength is the OPD (optical path difference) for each zone. That is why these lenses are sometimes referred to as "one wavelength Fresnel lenses".

These two examples indicate the difference between having the job done with a diffractive surface on a plane-parallel substrate and a combination of refractive and diffractive powers. To be able to reduce the numbers of zones from 1215 to 41 speaks for itself. Furthermore, it is clear from the results that diamond turning is not an economical method for producing lenses of the first kind in any volume. It is, however, a good way to make prototypes to demonstrate a principle in a timely fashion; because no lithographic masks, no molds or masters are required. Of course, there is not much room for any cutting tool radius. At the edge of the 12.5 mm diameter lens, the spacing of the zones is about 2.6  $\mu\text{m}$ . Therefore, the machining may have to be done by plunge cutting.

## 6. BROADBAND LENSES<sup>2,5,7</sup>

In addition to spherical aberration, a lens needs to be corrected for chromatic aberration if it is being considered for any broadband application.

To correct color, one takes advantage of the fact that the chromatic aberration of a diffractive element is opposite in sign when compared to the chromatic aberration of a refractive element as indicated in figure 1.

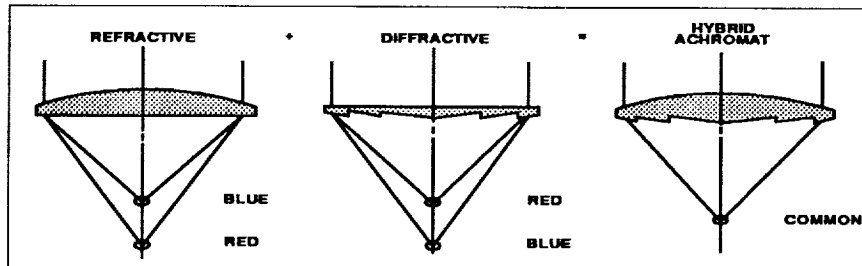


Figure 1. Principle of color correction with diffractive optics

$$\text{Power } \phi_R + \phi_D = \phi_{\text{TOTAL}}$$

$$\text{or } F = \frac{F_R F_D}{F_R + F_D} \quad (10)$$

To correct chromatic aberration, the following conditions must exist

$$F_D = (1 - v_R/v_D) F \quad (11)$$

$$\text{and } F_R = (1 - v_D/v_R) F \quad (12)$$

$$\text{with } v_R = \frac{N_0 - 1}{N_S - N_L} \quad \text{and} \quad \frac{\lambda_0}{\lambda_S - \lambda_L}$$

$v_R$  is called the Abbe number of refraction and  $v_D$  is the Abbe number of diffraction.  
 $v_D$  indicates that for the diffraction effects, the lens material is immaterial.  
 $\lambda_0$  is the center wavelength for which the index of refraction is  $N_0$ .  
 $\lambda_S, \lambda_L$  are the short and long limiting wavelengths of the spectral band.

### 6.1. THE ACHROMATIC SINGLET

An excellent summary of what can be achieved by combining refractive and diffractive powers in a single element to correct spherical and chromatic aberration is shown in figure 2.

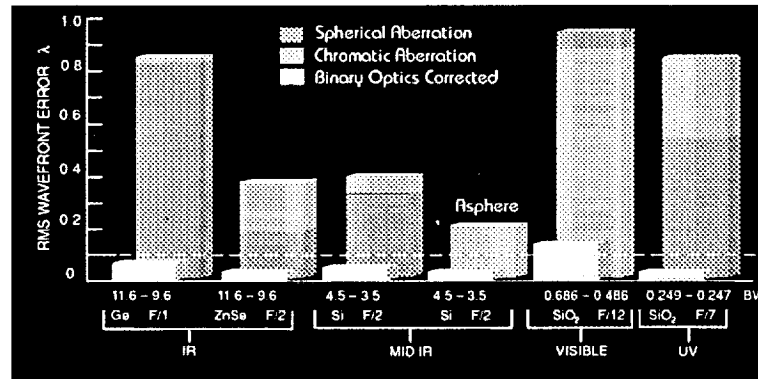


Figure 2. Examples of the chromatic and spherical aberration reduction possible by using a refractive/diffractive lens [With permission from Lincoln Laboratory<sup>2</sup>].

It can be seen clearly how the degree of correction is dependent on the lens material, the spectral region, and the relative aperture. For example, the F/1 germanium lens is overwhelmingly afflicted with spherical aberration and mildly affected by chromatic aberration over the 2 μm band width. On the other hand, the quartz lens applied in the visible spectrum over a band width of 0.2 μm, shows much chromatic and little spherical aberration. To achieve a reasonable correction, the relative aperture had to be increased to F/12.

It can also be seen how advantageous it is to use an aspheric surface for the elimination of spherical aberration. By superimposing the phase profile onto the asphere allows the other surface of the lens to be spherical. The preferred arrangement is to place the aspheric phase profile on the second surface for better environmental protection. The spherical front surface can be produced by conventional manufacturing processes if desired.

To find the first zone radius for such an achromatic singlet, the diffractive focal length is substituted into equation (4) to form

$$r_1 = \sqrt{2\lambda_0 (1 - v_R/v_D)} F \quad (13)$$

The total number of zones required is then

$$n_{TOT} = \frac{F}{8\lambda_0 (1 - v_R/v_D) (F/\#)^2} \quad (14)$$

Considering that the center wavelength for the 3 to 5  $\mu\text{m}$  region is 4  $\mu\text{m}$  and the diffractive Abbe number is -2 leads to very simple approximations.

$$r_1 \cong \frac{\sqrt{v_R F}}{15.8} \quad [r_1 \text{ and } F \text{ in mm}] \quad (15)$$

and

$$n_{\text{TOT}} \cong \frac{62 F}{v_R (F/\#)^2} \quad [F \text{ in mm}] \quad (16)$$

#### Summary for the 3 to 5 $\mu\text{m}$ region

Material	$v_R$	$r_1$	$n_{\text{TOT}}$
Silicon	235.5	1 $[\sqrt{F}]$	0.263 $[F/(F/\#)^2]$
Zinc Selenide	176.7	0.84	0.351
Zinc Sulfide	133.8	0.73	0.463
Germanium	104.8	0.65	0.592

( $r_1$  and  $F$  in mm)

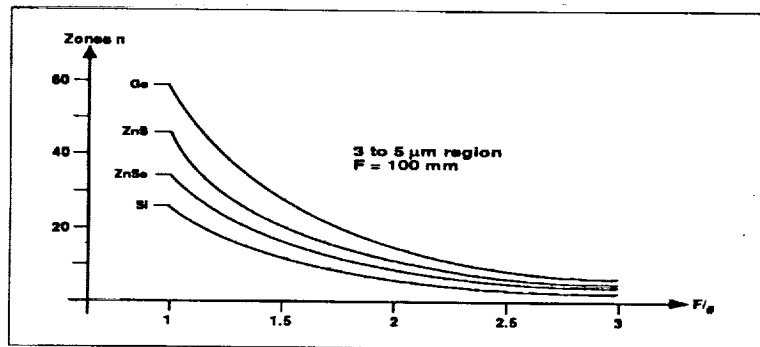


Figure 3. Number of zones as a function of  $F/\#$  for different materials

Example 3: A ZnSe lens with a relative aperture of  $F/1.5$  requires 16 zones. This is a reasonable low number for a 67 mm diameter diamond turned grating.

Figure 4 shows a 50 mm diameter diamond turned ZnS diffractive lens for the 3 to 5  $\mu\text{m}$  region. The narrowing of the zones towards the edge of the lens can clearly be seen.

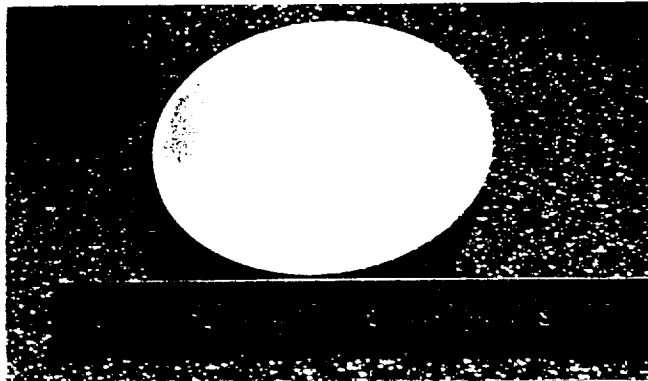


Figure 4. Diamond turned achromatic singlet

Similarly as for the mid IR region, one can summarize for the 8 to 12  $\mu\text{m}$  window, where  $\lambda_0 = 10 \mu\text{m}$  and  $\nu_r = -2.5$  :

$$r_1 \cong \frac{\sqrt{\nu_r} F}{11.2} \quad (17)$$

and

$$n_{\text{TOT}} \cong \frac{31 F}{\nu_r (F/\#)^2} \quad (18)$$

#### Summary for the 8 to 12 $\mu\text{m}$ region

Material	$\nu_r$	$r_1$	$n_{\text{TOT}}$
Germanium	863.0	$2.62 [\sqrt{F}]$	$0.036 [F/(F/\#)^2]$
Amir 3	109.8	0.94	0.282
Zinc Selenide	57.5	0.68	0.539

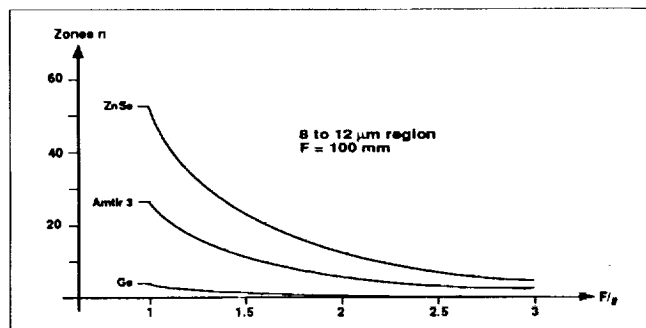


Figure 5. Number of zones as a function of F/# for different materials

One can see how effective germanium is in this region.

## 6.2. DIFFRACTION EFFICIENCY

It has been stated that the scalar theory used to predict diffraction efficiencies is overly optimistic. An extension to this theory was developed in early 1991 at the Lincoln Laboratory.<sup>8</sup> This extended scalar theory takes into account the ratio of the wavelength and the grating period. The equations developed show that when that ratio is very small -or in other words- if the period is much larger than the wavelength, the impact on the efficiency is negligible. This is the case for all the diamond turned optics discussed here. Therefore, only expressions based on the pure scalar theory will be applied for these pre-design considerations.

The grating efficiency referred to the first diffraction order is

$$\epsilon_1 = \left[ \frac{\sin \left[ \pi \left( \frac{\lambda_0}{\lambda} - 1 \right) \right]}{\pi \left( \frac{\lambda_0}{\lambda} - 1 \right)} \right]^2 \quad (19)$$

This yields, when integrated over a band width of  $\Delta \lambda = \lambda_L - \lambda_S$ , an approximated average efficiency of

$$\bar{\epsilon}_1 \cong 1 - \frac{\pi^2}{36} \left( \frac{\Delta \lambda}{\lambda_0} \right)^2 \quad (20)$$

It is very important to be aware of the efficiencies at the band width limits. Looking at the average value can be deceiving and can cause serious systems problems. This is best demonstrated by looking at the limits of the two spectral windows.

The average efficiency for the first order over the 3 to 5  $\mu\text{m}$  window is approximately 0.931, a relative large number. The efficiency at 5  $\mu\text{m}$  is only 0.875 and drops even further down to 0.684 at 3  $\mu\text{m}$ . For the 8 to 12  $\mu\text{m}$  window, the situation is somewhat better, but still of great concern for any given application. The average efficiency over this window is 0.956 with 0.912 at the long wavelength and 0.811 at the short one.

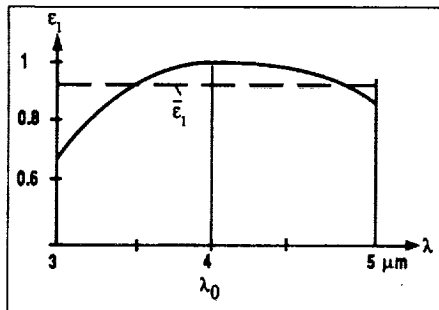


Figure 6

Diffraction efficiency over  
the 3 - 5  $\mu\text{m}$  region

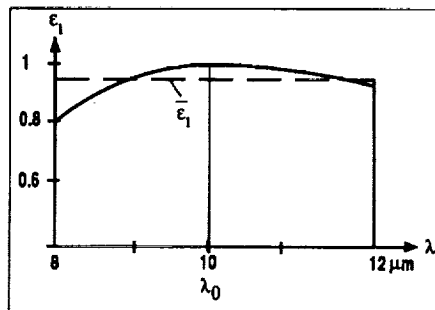


Figure 7

Diffraction efficiency over  
the 8 - 12  $\mu\text{m}$  region

It is worthwhile to mention that for some specific applications it may be desired to take advantage of this roll-off effect. An example may be a radiometric application which favors that the peak efficiency occurs at say  $4.5 \mu\text{m}$  ( detect ) with a lower transmission (diffraction efficiency) at say  $3.2 \mu\text{m}$  ( guard ). Figure 8 shows the efficiency distribution for this case.

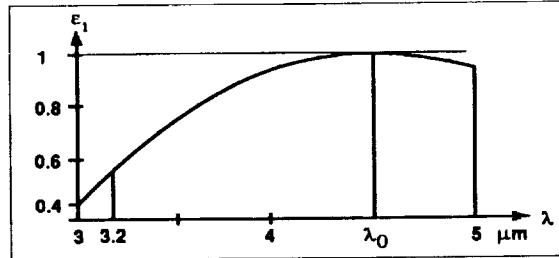


Figure 8. Blazed phase profile, for peaked efficiency at  $4.5 \mu\text{m}$

Another possibility for the efficiency distribution over the spectral band is to shift the center wavelength  $\lambda_0$  so that the efficiencies at both limiting wavelengths are equal. From equation (19) one can find by inspection that this occurs for the 3 to  $5 \mu\text{m}$  window when  $\lambda_0 = 3.75 \mu\text{m}$  and at  $\lambda_0 = 9.6 \mu\text{m}$  for the 8 to  $12 \mu\text{m}$  window.

As a general comment, one has to keep in mind that the energy not transmitted into the first diffraction order goes into other orders and must be treated as stray or scattered radiation.

### 6.3. SURFACE ROUGHNESS AND SCATTERING

The surface finish achievable with diamond turning is related to the radius of the cutting tool, the cutting feed rate, the stiffness of the machine and the material being machined.<sup>9,10</sup> Additional factors, such as coolant and others, apply as well. Surprisingly, the surface quality is quite insensitive to surface speed. That is confirmed by the fact that most of the diamond turning machines in use today do not have a continuously variable spindle speed which would be required to maintain a constant surface speed.

From the above parameters one can make some prediction about the expected surface finish.

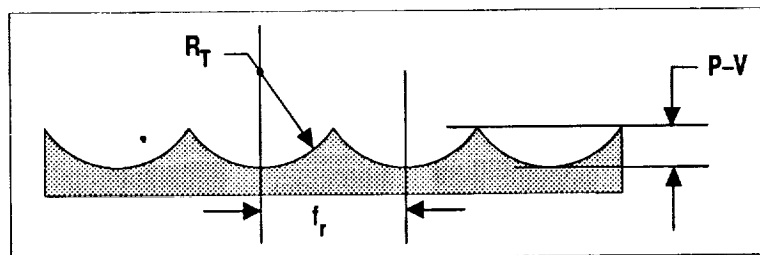


Figure 9. Theoretical Surface Finish

- $R_T$  = cutting tool radius
- $f_r$  = feed per revolution
- P-V = peak to valley surface roughness

From the figure it can easily be seen that

$$P-V = \frac{f_r^2}{8R_T} \quad (\text{theoretical}) \quad (21)$$

Typical values are  $R_T = 0.030$  inch and  $f_r = 0.0003$  inch per revolution. This yields a P-V finish of  $0.375 \mu\text{inch}$  or  $95 \text{ \AA}$ . Surface roughness is usually stated in RMS and a reasonable factor between P-V and RMS is 6. This is also a good factor to be considered for the influence on the finish caused by the limited machine stiffness and other factors mentioned earlier. Therefore, since these two factors cancel each other, a more realistic surface roughness prediction is

$$\text{RMS} \cong \frac{f_r^2}{8R_T} \quad (\text{more realistic}) \quad (22)$$

A surface roughness of  $80$  to  $120 \text{ \AA}$  is typical. It varies, depending on the material being machined. The roughness profile of an exceptionally smooth diamond turned surface is shown in figure 10. It also confirms the P-V to RMS ratio of approximately 6.

RMS: 6.33 nm  
RA: 5.07 nm  
P-V: 38.4 nm

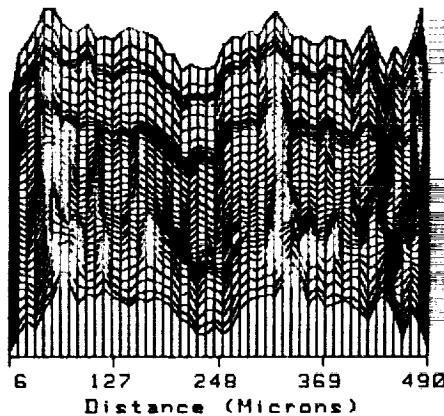


Figure 10. Roughness profile of a diamond turned surface

The roughness of a surface is another source for energy through-put reduction. This is due to scattering. To assess the magnitude of this loss, the relation for TIS (total integrated scatter) developed by the Naval Weapons Center<sup>11</sup> is being applied:

$$\text{TIS} = \left[ \frac{4\pi \delta}{\lambda_0} \right]^2 \quad (23)$$

where  $\delta$  is the RMS surface roughness and  $\lambda_0$  is the wavelength of interest. For a roughness of  $95 \text{ \AA}$  and a wavelength of  $4 \mu\text{m}$ , TIS is approximately 0.1%, which is negligible for these predesign considerations.

#### 6.4. BLOCKAGE OF RADIATION CAUSED BY DIAMOND TOOL RADIUS

The radius of the cutting tool forms an annulus at the transition from one zone to another. This causes an energy blockage which is illustrated in figure 11.

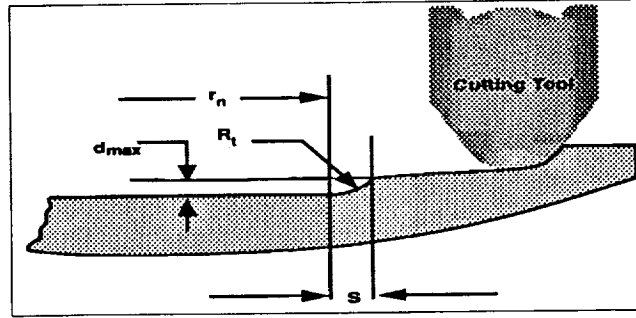


Figure 11. Zone transition geometry, showing the cutting tool radius effect

The area of the blockage or shadow formed by one ring is

$$A_{sr} \cong 2\pi r_n s \quad (24)$$

The total shadow is therefore

$$A_s \cong 2\pi s \sum_1^{n_{TOT}-1} r_n \quad (25)$$

With  $s = \sqrt{2R_t d_{max}}$  and some additional substitution one can determine that

$$A_s = D\pi \sqrt{\frac{2R_t \lambda_0}{(N-1) n_{TOT}}} \sum_1^{n_{TOT}-1} \sqrt{n} \quad (26)$$

Over the total lens area  $\frac{D^2\pi}{4}$ , the loss due to this shadowing effect becomes

$$L = \frac{4(F/\#)}{F} \sqrt{\frac{2R_t \lambda_0}{(N-1) n_{TOT}}} \sum_1^{n_{TOT}-1} \sqrt{n} \quad (27)$$

with  $N$  being the index of refraction of the lens material.

Example 4:

The ZnSe lens from example 3, with  $N = 2.433$ ,  $F = 100$  mm,  $F/\# = 1.5$ ,  $\lambda_0 = 4$   $\mu\text{m}$ , has 16 zones. With a tool radius of 0.030 inch, the transmission loss due to the tool caused shadowing is approximately 4%. This could be reduced to 2% if the tool radius would be decreased to .010 inch. The surface roughness would go up to 286 Å. To maintain the 95 Å surface roughness, the tool feed would have to be slowed down to 0.00017 inch per revolution. This in turn would approximately double the machining time and therefore increase the cost of the lens. Again, these are all considerations to be taken into account at the preliminary project stages.

Judging from all this, it becomes clear that the optical performance limitation of broad band lenses is not so much dependent on the method of manufacturing but on the roll-off effects in the diffraction efficiency at the upper and lower wavelength limits.

6.5. COMMENTS TO USABLE BAND WIDTH

Looking at equation (20) differently provides a better picture of the relationship between the usable band width for a desired efficiency. It also shows clearly the advantage of using diffractive lenses at longer wavelengths.

$$\Delta \lambda \cong \frac{6 \lambda_0}{\pi} \sqrt{1 - \bar{\epsilon}_1} \tag{28}$$

One can see that for an average efficiency of 99% the band width in the visible can only be 0.1  $\mu\text{m}$ . For the mid IR this increases to 0.76  $\mu\text{m}$  and broadens to 1.91  $\mu\text{m}$  for the long wavelengths region. This has been already demonstrated in principle in figure 2.

7. THE AIR SPACED ACHROMATIC DOUBLET

A Petzval type lens has been chosen for these predesign considerations for an air spaced doublet. The uniqueness of such a lens simplifies the discussion and provides a good starting point for a well performing IR objective.

The assumptions for this Petzval objective are:<sup>12</sup>

$F_A = 2F$ ,  $F_B = F$ ,  $d = F$ . With this, the  $BFL = F/2$ . The stop is at the front element which is the hybrid lens. Both lens elements are from the same material. The symbols and relations are identified in figure 12.

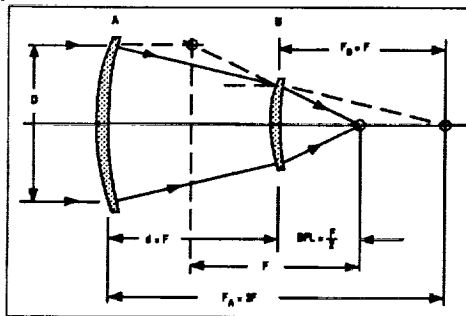


Figure 12. Relations for the basic Petzval objective

Using the same basic approach as for the singlet and applying the general 3rd order expressions for separated thin lenses, the following approximations can be developed.

$$r_1 = \sqrt{\frac{8}{3} \lambda_0 (1 - v_R/v_D)} F \quad (29)$$

and

$$n_{TOT} = \frac{3F}{32 \lambda_0 (1 - v_R/v_D) (F/\#)^2} \quad (30)$$

These expressions, simplified for the two spectral windows, are

### 3 to 5 $\mu\text{m}$ window

First zone radius

$$r_1 \underset{3-5}{\cong} \frac{1}{13.7} \sqrt{v_R} F \quad (31)$$

Total number of zones required

$$n_{TOT} \underset{3-5}{\cong} \frac{47 F}{v_R (F/\#)^2} \quad (32)$$

### 8 to 12 $\mu\text{m}$ window

First zone radius

$$r_1 \underset{8-12}{\cong} \frac{1}{9.7} \sqrt{v_R} F \quad (33)$$

Total number of zones required

$$n_{TOT} \underset{8-12}{\cong} \frac{23.5 F}{v_R (F/\#)^2} \quad (34)$$

Looking at the same materials as before we can summarize for the two regions

### Petzval for the 3 to 5 $\mu\text{m}$ region

Material	$r_1$	$n_{TOT}$
Silicon	1.1 [ $\sqrt{F}$ ]	0.200 [ $F/(F/\#)^2$ ]
Zinc Selenide	1	0.266
Zinc Sulfide	0.84	0.351
Germanium	0.75	0.448

For Zn Se,  $F/1.5$ ,  $F = 100$  mm:  $r_1 = 10$  mm and  $n_{TOT} = 12$  zones.

### Petzval for the 8 to 12 $\mu\text{m}$ region

Material	$r_1$	$n_{\text{TOT}}$
Germanium	3 [ $\sqrt{F}$ ]	0.027 [ $F/(F\#)^2$ ]
Amtir 3	1.1	0.213
Zinc Selenide	0.78	0.407

The remarks made earlier about diffraction efficiency, surface roughness and the shadowing effects remain of course valid for any diamond turned diffractive element in an optical train.

Figure 13 shows such a Petzval objective which replaced a triplet.<sup>5,13</sup> Its focal length is 84 mm and its relative aperture is 1. The elements are made from germanium. It is being used in the 8 to 12  $\mu\text{m}$  band with a staring detector array in the focal plane.

From the table above it can be seen that only 3 zones are required to correct the chromatic aberration. Spherical aberration was eliminated by aspherizing the first surface. The objective has an excellent performance over a total field of view of  $8^\circ$ . The 80% blur spot was calculated to be close to the diffraction limit. The measured one was somewhat larger.

A similar Petzval objective for 3 to 5  $\mu\text{m}$  has been designed and manufactured with silicon elements. It is being tested now. Because Silicon is difficult to diamond turn, another objective with the same focal length of 50 mm has been designed, using ZnSe for the diffractive hybrid front element and a Si lens in the rear. The expected 80% blur spot size is 32  $\mu\text{m}$  over a total flat field of  $11.5^\circ$ . These lenses have been optimized with CODE V and OSLO. The resulting phase profiles obtained with these computer programs confirm the validity of the presented redesign approximations.

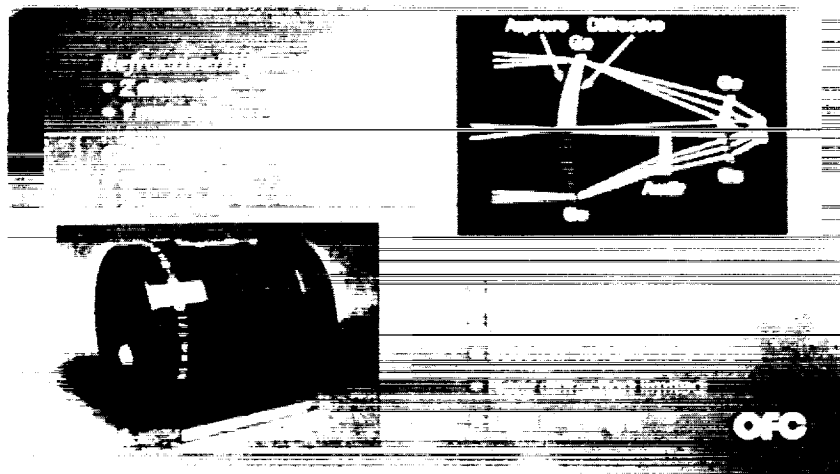


Figure 13. Comparison of a diffractive doublet which replaced a conventional triplet.

## 8. CONCLUSIONS

From the presented material one can conclude that for reasonable focal lengths the number of diffraction zones required to correct chromatic aberration is relatively small for hybrid lenses applied in the two most common IR windows. This makes it possible and very practical to use the process of diamond turning. Beyond the singlet and the doublet there exists a wide range of opportunities, limited only by ones imagination, for the application of these hybrid components. These diffractive elements are an additional tool for the lens designer. They are of particular value for a system when reduction in weight, cost and size is of interest.

## 9. ACKNOWLEDGEMENT

We thank the team from the Lincoln Laboratory, Wilfrid Veldkamp, Gary Swanson, and Robert Knowlden, for their continued support and stimulation. We also thank the personnel from Optical Research Associates and Sinclair Optics for their efforts in upgrading and fine tuning their computer programs for HOEs.

## 10. REFERENCES

(a limited list)

1. Frost & Sullivan, Inc., "Binary Optics, A Technology Impact Report," Summer 1991.
2. G. J. Swanson, "Binary Optics Technology: The Theory and Design of Multilevel Diffractive Optical Elements," Technical Report 854, Lincoln Laboratory 14 August 1989.
3. F. P. Shvartsman, "Dry Photopolymer Embossing: Novel Photoreplication Technology for Surface Relief Holographic Optical Elements," Proc. SPIE Vol.1507, 1991.
4. P. P. Clark and C. Londono, "Production of Kinoforms by Single Point Diamond Machining," Optics News, December 1989.
5. M. J. Riedl and J. T. McCann, "Analysis and Performance Limits of Diamond Turned Diffractive Lenses for the 3-5 and 8-12 Micrometer Regions," SPIE Critical Review, Vol. CR 38, April 1991.
6. M. J. Riedl, "The Single Thin Lens as an Objective for IR Imaging Systems," Electro-optical Systems Design, Nov. 1974.
7. D. Faklis and G. M. Morris, "Optical Design with Diffractive Lenses" Photonics Spectra, Nov. and Dec. 1991.
8. G. J. Swanson, "Binary Optics Technology: Theoretical Limits on the Diffraction Efficiency of Multilevel Diffractive Optical Elements," Technical Report 914, Lincoln Laboratory, 1 March 1991.
9. G. M. Sanger, "The Precision Machining of Optics," in "Applied Optics and Optical Engineering, Volume X," Academic Press, 1987.
10. R. A. Clark, "Design and Specification of Diamond Turned Optics," SPIE Critical Review, Vol. CR 38, April 1991.
11. J. M. Bennett and L. Mattsson, "Introduction to Surface Roughness and Scattering," Optical Society of America, Washington D.C. 1989.
12. W. J. Smith, "Modern Optical Engineering," second edition, page 427, McGraw-Hill 1990
13. T. A. Fritz and J. A. Cox, "Diffractive Optics for Broad Band Infrared Imagers: Design Examples" in Holographic Optics: Optically and Computer Generated, Proc. SPIE Vol. 1052, 1989.
14. D. C. Sinclair, "Designing Diffractive Optics using the Sweatt Model," Sinclair Optics Design notes Vol. 1, No. 1, Winter 1990.
15. I. Cindrich, "Holographic Optics: Design and Applications, Proc. SPIE, Vol. 883, Jan. 1988.
16. G. N. Lawrence, "International Lens Design Conference," Proc. SPIE, Vol. 1354, June 1990.
17. D. A. Buralli and G. M. Morris, "Design of Wide Field Diffractive Landscape Lens," Applied Optics, Vol. 28, No. 18, 15 Sept. 1989.
18. D. A. Buralli, G. M. Morris, and J.R. Rogers, "Optical Performance of Holographic Kinoforms," Applied Optics, Vol. 28, No. 5, 1 March 1989.
19. G. J. Swanson and Veldkamp "Diffractive Optical Elements for use in Infrared Systems," Optical Engineering, Vol. 28, No. 6, 1989.
20. J. Jahns and S. J. Walker, "Two-dimensional Array of Diffractive Microlenses fabricated by Thin Film Deposition" Applied Optics, Vol. 29, No. 7, 1 March.

21. T. Stone and N. George, "Hybrid Diffractive-Refractive Lenses and Achromates," *Applied Optics*, Vol. 27, No. 14, 1 July 1988.
22. T. J. McHughes and D. A. Zweig, "Recent Advances in Binary Optics" in Holographic Optics: Optically and Computer Generated, Proc. SPIE, Vol. 105, 1989.
23. S. H. Lee, "Recent Advances in Computer Generated Holographic Applications," *Optics & Photonic News*, July 1990.
24. W. C. Sweatt, "Describing Holographic Optical Elements as Lenses," *JOSA* 67 (6) 803-808 (1977).
25. W. C. Sweatt, "Mathematical Equivalence between a Holographic Optical Element and an Ultra-high Index Lens," *JOSA* 69 (3) 486-387 (1979).

